Probing the Cosmic Neutrino Background through Parametric Fluorescence

Guo-yuan Huang[1,*] and Shun Zhou[2,3,†]
[1]School of Mathematics and Physics, China University of Geosciences, 430074 Wuhan, China
[2]Institute of High Energy Physics, Chinese Academy of Sciences, Beijing 100049, China
[3]School of Physical Sciences, University of Chinese Academy of Sciences, Beijing 100049, China

(Received 10 August 2025; revised 22 November 2025; accepted 5 February 2026; published 24 February 2026)

We point out that relic neutrinos from the Big Bang may induce the parametric fluorescence in atomic or molecular systems, which offers a novel way to discover cosmic neutrino background. By coherently scattering with molecular energy levels, a massive neutrino can spontaneously "decay" into a lighter neutrino and an infrared signal photon; i.e., $\nu_i + M \to \nu_j + \gamma_S + M$, where the molecular state M remains unchanged after the scattering. Because the amplitudes of different radiants are matched in phase, the rate is coherently enhanced and proportional to the squared density of ambient dipoles. When the energy transfer from neutrinos coincides with the energy-level difference, the fluorescence will be on resonance. Near the resonance, the rate is proportional to the square of the coherence time T_c of the ensemble. For a nominal target volume of 5 m^3 (or 5 cm^3), the signal rate can reach 1 yr^{-1} for $T_c = 10$ ns (or $T_c = 10$ μs). This event rate appears to be very promising in consideration of an even longer coherence time that is achievable in solid systems.

DOI: 10.1103/f4zt-bbzv

Introduction—The Big Bang theory predicts the existence of both cosmic microwave background (CMB) and cosmic neutrino background (CνB). While the CMB has been firmly observed and serves as a powerful probe of the early Universe [1], the CνB, formed one second after the Big Bang, has yet to be detected. To date, the most promising method for observing these relic neutrinos is through the inverse beta-decay process, initially proposed by S. Weinberg in 1962 [2]. Nevertheless, the PTOLEMY project, currently under development with tritium targets, still faces significant challenges before its practical feasibility can be confirmed [3–7]. An alternative approach to relic neutrino detection is to observe the mechanical recoils from their coherent scattering on a macroscopic object [8–25]. However, while the event rate for coherent scattering can be enhanced by a factor of the Avogadro constant, the resulting sub-eV recoil is averaged across all the atoms in the target ensemble, posing a fundamental challenge for detecting those elusive relics. For instance, for the mechanical recoil, the resultant acceleration is fifteen orders of magnitude below the most advanced measurements [24].

*Contact author: huangguoyuan@cug.edu.cn
†Contact author: zhoush@ihep.ac.cn

Published by the American Physical Society under the terms of the Creative Commons Attribution 4.0 International license. Further distribution of this work must maintain attribution to the author(s) and the published article's title, journal citation, and DOI. Funded by SCOAP³.

In this Letter, we investigate a novel phenomenon of the coherent parametric fluorescence of relic neutrinos in cold molecular (or atomic) systems. A schematic plot for the process is shown in the left panel of Fig. 1. By collectively interacting with molecular dipoles, the parametric fluorescence $\nu_i + M \to \nu_j + \gamma_S + M$ with neutrino masses $m_i > m_j$ will be induced, a spontaneous process that is unlikely to occur without the presence of the medium. Microscopically, neutrinos are scattering with dipoles in the medium through their coupling to electrons, and the process is coherent for the ensemble because dipoles in the medium remain unmodified after the scattering.

The medium of our concern is characterized by generic electric or magnetic dipoles $\boldsymbol{d}$ of Avogadro's number. Those dipoles radiate collectively if phases of their scattering amplitudes are matched. The microscopic process of the parametric fluorescence is described by the diagram on the

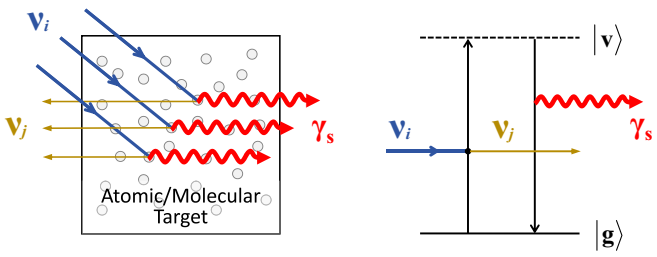


FIG. 1. Schematic diagrams for the parametric fluorescence induced by massive neutrinos, which collectively interact with molecular (or atomic) dipoles in the medium.

right panel of Fig. 1. We assume that all the molecules in the system are in their ground state $|\mathrm{g}\rangle$, by maintaining a low medium temperature. Neutrino fields couple to the dipole system via the four-fermion interaction, while photons couple to the system via the electric (or magnetic) dipole interaction $\boldsymbol{d}\cdot\boldsymbol{\mathcal{E}}$ (or $\boldsymbol{d}\cdot\boldsymbol{\mathcal{B}}$). When a heavier relic neutrino ν_i passes through this medium, it can first excite the dipole to a virtual state $|\mathrm{v}\rangle$ and be converted to a lighter neutrino ν_j. The virtual energy level jumps back to the ground state by radiating a photon γ_S. If the scattering amplitude contributed by each radiant of the medium is represented by $\mathcal{M}_r$, then the total amplitude will be

$$\mathcal{M}_\mathrm{tot}=\sum_{r=1}^{N}\mathcal{M}_r\cdot\mathrm{e}^{\mathrm{i}(\boldsymbol{p}_i-\boldsymbol{p}'_j-\boldsymbol{k})\cdot\boldsymbol{x}_r}. \tag{1}$$

Here, N refers to the total number of dipoles in the medium, $\boldsymbol{x}_r$ is the position of the dipole radiant $\boldsymbol{d}_r$, and $\boldsymbol{p}_i$, $\boldsymbol{p}'_j$ and $\boldsymbol{k}$ are the momenta of the initial neutrino, the outgoing neutrino and the signal photon, respectively. When the phase matching condition $\boldsymbol{q}\equiv\boldsymbol{p}_i-\boldsymbol{p}'_j-\boldsymbol{k}=0$ is satisfied (for a uniform medium), different dipoles will radiate in phase and the event rate will receive an enhancement of the squared density.

Since the medium remains unchanged after the fluorescence process, the kinematics for the process $\nu_i\to\nu_j+\gamma_\mathrm{S}$ is similar to radiative neutrino decays in vacuum. The energy of the signal photon will be affected by the neutrino mass ordering, which will hopefully be determined within a few years independently by JUNO [26,27] and DUNE [28,29]. For concreteness, we take the lightest neutrino mass to be vanishing, and thus the heaviest neutrino mass will be $m_i\approx 0.05$ eV. In the case of normal mass ordering (NO), the heaviest neutrino will be ν_3, and the photon energy for $\nu_3\to\nu_1$ or ν_2 should be about $\omega\sim m_3/2\approx 0.025$ eV, which falls within the far-infrared range of light. In the case of inverted mass ordering (IO), the transition from the heaviest neutrino will generate a photon with energy about $\omega\sim 0.025$ eV (for $\nu_2\to\nu_3$) or $\omega\sim m_2/2\approx 7.5\times10^{-4}$ eV (for $\nu_2\to\nu_1$), the latter of which corresponds to the microwave frequency. While it might be challenging to detect single quantum of microwave, one-photon detection at far-infrared frequencies should be feasible with modern or near-future technologies [30], such as superconducting tunnel junction sensors [31], kinetic inductance detectors [32], quantum capacitance detectors [33], etc. Therefore, we shall focus on the representative scenario of $\nu_3\to\nu_1$ in the NO case.

In nonlinear optics, a laser beam γ_P pumping into certain crystals can be efficiently converted into two photon beams γ_S and γ_I at lower energies by coherently scattering with dipoles in the crystal. This process $\gamma_\mathrm{P}\to\gamma_\mathrm{S}+\gamma_\mathrm{I}$ is referred to as the spontaneous parametric down-conversion (SPDC) [34–37], arising from the nonlinear electric susceptibility of the material. The conversion efficiency relies largely on detailed configurations of atoms or molecules, and can be calculated from first principles of quantum mechanics. The most intriguing aspect of this well-established phenomenon is that resonance enhancement occurs when the frequency of the radiation aligns with the corresponding energy-level difference [34,35]. The fluorescence process induced by neutrinos is similar to the pure electromagnetic scenario. This phenomenon should be distinguished from the soft photon emission due to coherent scattering of neutrinos with free electron gas [16] and very off-shell scatterings with binding electrons for neutrinos at higher energies [38].

Parametric fluorescence rate for massive neutrinos—The fluorescence processes can be interpreted as the dipole radiation of a polarized medium under the perturbation of external fields. As shown in the right panel of Fig. 1, the essence is to have a two-level system with a ground state $|\mathrm{g}\rangle$ and a virtual state $|\mathrm{v}\rangle$. The system is initially prepared in the ground state $|\mathrm{g}\rangle$. Through the virtual state $|\mathrm{v}\rangle$, the scattering process then reads $\nu_i+|\mathrm{g}\rangle\to\nu_j+|\mathrm{g}\rangle+\gamma$.

The essential way to calculate the fluorescence rate is to determine the Hamiltonian density for the effective neutrino-photon coupling induced by dipoles. In nonlinear optics, there is a standard procedure to extract the Hamiltonian density for the electromagnetic couplings [34–36], by calculating the electric or magnetic polarization (i.e., the induced dipole moment per volume) $\boldsymbol{P}$ in response to the field perturbation. The polarization reflects the strength of the medium optical response when an external field is applied. The Hamiltonian density describing this response can be straightforwardly obtained with $\mathcal{H}_\mathrm{eff}=-\boldsymbol{P}\cdot\boldsymbol{\mathcal{E}}$ or $\mathcal{H}_\mathrm{eff}=-\boldsymbol{P}\cdot\boldsymbol{\mathcal{B}}$ depending on whether this polarization is electric or magnetic (see Supplemental Material Sec. I [39]). The effective Hamiltonian density and transition matrix for neutrino interactions can be derived in a similar manner.

Neutrino current can induce both the M1 and E1 transitions (see Ref. [39] Sec. II). In our context, the M1 transition is preferred because its neutrino-induced current is of order 1, while the corresponding current in the E1 case is suppressed by the Bohr radius. Hence, in the following we should focus on the M1 transition, and the result for the E1 case will also be presented in Ref. [39] Sec. III. In general, the quantum state of the system can be described as a superposition of discrete energy levels,

$$|\Psi(t)\rangle=C_\mathrm{g}(t)|\mathrm{g}\rangle+\sum_\mathrm{v}C_\mathrm{v}(t)|\mathrm{v}\rangle, \tag{2}$$

where C_g and C_v are coefficients of the ground state and various excited states, respectively. The initial state is set to be $|\Psi_0\rangle=|\mathrm{g}\rangle$.

For a two-level system connected via the M1 transition, the relevant Hamiltonian describing the neutrino and photon interactions is represented by Eq. (9) in Ref. [39]. In this case, the M1 transition corresponds to a flip in the electron

spin. Those two spin configurations can feature different energies in the presence of couplings to the orbital angular momentum or a static magnetic field. The coefficient for $|\mathrm{v}\rangle$ under the perturbation of neutrino fields reads,

$$C_{\mathrm{v}}^{(1)}(t) = \frac{G_{\mathrm{F}} C_{ij}}{\sqrt{2}} \frac{\hat{\boldsymbol{j}}_{ij} \cdot \boldsymbol{\sigma}_{\mathrm{vg}}}{E_{\mathrm{vg}} + E'_j - E_i} \mathrm{e}^{\mathrm{i}(E_{\mathrm{vg}} + E'_j - E_i)t}, \quad (3)$$

where G_{F} is the Fermi constant and $C_{ij} \equiv U^*_{ei} U_{ej}$ $(i \neq j)$ with U being the Pontecorvo-Maki-Nakagawa-Sakata (PMNS) matrix, E_{vg} is the energy difference between $|\mathrm{v}\rangle$ and $|\mathrm{g}\rangle$, $\hat{\boldsymbol{j}}_{ij}$ denotes the neutrino current operator, and $\boldsymbol{\sigma}_{\mathrm{vg}} \equiv \langle \mathrm{v}|\boldsymbol{\sigma}|\mathrm{g}\rangle$ with $\boldsymbol{\sigma}$ being the Pauli matrices. The polarization can be obtained similar to the pure electromagnetic case, and we present the resultant effective Hamiltonian density as

$$\mathcal{H}^{\mathrm{M1}}_{\nu\nu\gamma} = -\frac{G_{\mathrm{F}} C_{ij}}{\sqrt{2}} \frac{n_d [\hat{\boldsymbol{j}}_{ij} \cdot \boldsymbol{\sigma}_{\mathrm{vg}}][\boldsymbol{d}^*_{\mathrm{vg}} \cdot \boldsymbol{\mathcal{B}}(\boldsymbol{k})]}{E_{\mathrm{vg}} + E'_j - E_i} \times \mathrm{e}^{\mathrm{i}(\omega + E'_j - E_i)t} + \mathrm{H.c.}, \quad (4)$$

where $n_d \sim N_{\mathrm{A}}\ \mathrm{cm}^{-3}$ represents the number density of atomic or molecular dipoles in a solid with $N_{\mathrm{A}} \approx 6.02 \times 10^{23}$ being the Avogadro constant. The temporal phase explicitly shown implies the energy conservation. Other than the temporal phase, $\mathcal{H}^{\mathrm{M1}}_{\nu\nu\gamma}$ also carries a spatial phase in field operators, namely $\exp[\mathrm{i}(\boldsymbol{p}_i - \boldsymbol{p}'_j - \boldsymbol{k}) \cdot \boldsymbol{x}_r]$ as in Eq. (1). For a uniform medium, after integrating over the target volume this phase will result in the delta function $\delta^{(3)}(\boldsymbol{p}_i - \boldsymbol{p}'_j - \boldsymbol{k})$, which imposes the phase-matching condition (identical to the momentum conservation in vacuum) for the process to be coherent.

The transition matrix for $\nu_i \to \nu_j \gamma$ is obtained by an integration $\mathrm{i}T = -\mathrm{i} \int_{-\infty}^{\infty} \mathrm{d}^4 x \langle \boldsymbol{p}'_j, \boldsymbol{k}|\mathcal{H}_{\nu\nu\gamma}|\boldsymbol{p}_i\rangle$. For the uniform material, the kinematics of the transition is analogous to the case of the decay of nonrelativistic neutrinos in vacuum, and the decay products ν_j and γ will be back to back. Following the standard formula, the differential decay rate in the rest frame of ν_i with respect to the photon outgoing direction is

$$\frac{\mathrm{d}\Gamma}{\mathrm{d}\Omega_\gamma} = \int \mathrm{d}|\boldsymbol{k}| \frac{\boldsymbol{k}^2 |\mathcal{M}|^2}{32\pi^2 m_i E'_j \omega} \delta(\omega + E'_j - E_i). \quad (5)$$

The integration over the delta function will generate a dimensionless factor $D_k \equiv 1/[\mathrm{d}(\omega + E'_j - E_i)/\mathrm{d}|\boldsymbol{k}|]$. The actual value of D_k relies on neutrino masses as well as the dispersion relation of photons in medium. For $\nu_3 \to \nu_1$ with a nearly massless ν_1 in the NO case, the energy of daughter particles just takes $E'_1 = \omega = m_3/2$, assuming the photon dispersion relation in vacuum. The value of D_k is just 2 in this case. The in-medium effect causes the energy of the signal photon to deviate from $m_3/2$, which will be discussed later.

We explicitly perform the angular integration, arriving at the rate

$$\Gamma \approx \frac{G_{\mathrm{F}}^2 |U^*_{ei} U_{ej}|^2}{2\pi} \frac{f_\theta^{\mathrm{M1}} n_d^2 |\boldsymbol{d}_{\mathrm{vg}}|^2 D_k}{(E_{\mathrm{vg}} + E'_j - E_i)^2 + \gamma_{\mathrm{vg}}^2/4} \frac{|\boldsymbol{k}|^4}{\omega}, \quad (6)$$

where $f_\theta^{\mathrm{M1}} \sim \mathcal{O}(1)$ is the form factor depending on the polarization of magnetic dipoles. The outgoing neutrino is taken to be relativistic in Eq. (6). The damping rate $\gamma_{\mathrm{vg}} \equiv T_{\mathrm{c}}^{-1}$ accounts for all factors that can affect the timescale of coherent accumulation of $|\mathrm{v}\rangle$, where T_{c} denotes the overall coherent timescale. When $E_{\mathrm{vg}} = E_i - E'_j$ is satisfied, the transition will be on resonance, and the rate will approximately be $\Gamma \sim G_{\mathrm{F}}^2 n_d^2 |\boldsymbol{d}_{\mathrm{vg}}|^2 |\boldsymbol{k}|^3 T_{\mathrm{c}}^2$ with $|\boldsymbol{d}_{\mathrm{vg}}| \sim e/m_e$ (i.e., the Bohr magneton) being the magnetic dipole moment. We notice that T_{c} is a key parameter for our rate estimation. The coherence time is mainly contributed by the spontaneous decay lifetime T_1 of $|\mathrm{v}\rangle$ and the pure dephasing time T_ϕ, according to the convention $T_{\mathrm{c}}^{-1} = T_1^{-1} + T_\phi^{-1}$ [52]. For energy splittings of $\mathcal{O}(25\ \mathrm{meV})$, the decay lifetime $T_1 \sim 1/(d_{\mathrm{vg}}^2 E_{\mathrm{vg}}^3)$ is relatively long (e.g., 120 s for M1 and 6 ms for E1 transitions), implying that coherence is mainly limited by the dephasing time T_ϕ arising from stochastic dipole-environment interactions. Over the past decades, substantial AMO advances have demonstrated spin coherence times in solids controllable at the $\mathcal{O}(10\ \mathrm{ms})$ level and even longer [53–59], highlighting the potential for achieving long-lived coherence in such systems.

The resonance enhancement also suggests that molecular materials are ideal target candidates, as their energy-level differences typically fall within the infrared range. In an ideal case that the incoming neutrino flux with a density $n_{\nu_i} \approx 112\ \mathrm{cm}^{-3}$ (including both neutrinos and antineutrinos) can satisfy the resonance condition, the event rate $R = n_{\nu_i} V \Gamma$ in a material target of volume V will roughly be given by

$$R_{\nu_3 \to \nu_1} \sim 1\ \mathrm{yr}^{-1}\ (V = 5\ \mathrm{m}^3, T_{\mathrm{c}} = 10\ \mathrm{ns}), \quad (7)$$

$$R_{\nu_3 \to \nu_1} \sim 8\ \mathrm{yr}^{-1}\ (V = 40\ \mathrm{cm}^3, T_{\mathrm{c}} = 10\ \mu\mathrm{s}), \quad (8)$$

assuming a resonance energy of $E_{\mathrm{vg}} = 0.025$ eV. Due to its T_{c}^2 dependence, the event rate appears highly promising if a long coherence time can be achieved, and a coherence time of 10 μs should be well achievable with existing techniques [53–57], particularly at low temperatures. Recall that in the case of Majorana neutrinos, the overall event rate will be doubled.

A condition for achieving the resonance rate in Eqs. (7) and (8) seems to have a highly monoenergetic neutrino flux that matches the energy level. Relic neutrinos with a

temperature 1.95 K in the Milky Way exhibit a momentum dispersion of order $\Delta p \sim 10^{-4}$ eV, leading to a tiny energy spread of order $\Delta E_3 \approx \Delta p^2/(2m_3) \sim 10^{-6}$ eV for the incoming nonrelativistic neutrinos. The corresponding timescale of the energy spread is on the order of 1 ns. Nevertheless, the actual resonance condition $E_{\rm vg} = E_3 - E_1'$ imposes stricter requirements, even if E_3 is already quite monoenergetic. Because the outgoing neutrino and photon are both ultrarelativistic for $\nu_3 \to \nu_1\gamma$ with $E_1' \approx |\boldsymbol{p}_1'|$ and $\omega = k$, this momentum spread actually results in a spread of comparable magnitude $\Delta(E_3 - E_1') \sim 10^{-4}$ eV. This energy spread will limit the resonance enhancement, because only a small portion of the neutrino flux ($\sim \gamma_{\rm vg}/\Delta p$ for $\Delta p \gg \gamma_{\rm vg}$) can cover the resonance peak. Thus, the average decay rate seems to be capped at $\Gamma \sim G_{\rm F}^2 n_{\boldsymbol{d}}^2 |\boldsymbol{d}_{\rm vg}|^2 \omega^3/(\gamma_{\rm vg}\Delta p)$. In this case, to reach the event rate of 1 yr^{-1}, a coherence timescale of 4 ms is required for the target volume $V = 40$ cm^3.

The discussions so far have not accounted for in-medium effects, which can alter photons' dispersion relation, thus affecting our rate estimates. This is unavoidable for applying our results to realistic detection, as resonance, which is our region of interest, typically strongly modifies the refractive index. Remarkably, we find that including the in-medium effect is not harmful and can even help by reducing the impact of relic neutrinos' momentum spread. The key is the slow-light phenomenon well recognized in modern quantum optics [60–62], which can render the outgoing photon effectively nonrelativistic with a reduced group velocity as $\mathcal{O}(10)$ m/s or even lower [57,63,64]. The group velocity is connected to photons' dispersion curve through $v_{\rm g} = {\rm d}\omega/{\rm d}k$. With this effect, we find that the energy spread can be controlled within $\Delta(E_3 - E_1') \sim (10^{-4} \cdot v_{\rm g})$ eV.

Interestingly, the slow light intrinsically occurs in the vicinity of the resonance [62]. This is unsurprising, as most slow-light schemes rely on photon scattering with some resonant structure of the medium, either discrete energy levels or photonic resonators [61]. The reduced group velocity arises from the resonant energy transfer between photons and other modes, such as the polarization of the nonrelativistic medium.

In Fig. 2, we show the dispersion curve for a two-level system, with detailed parameters provided in the caption. For illustration, we consider an energy level separation of $E_{\rm vg} = 10$ meV. Near the resonance energy, the dispersion splits into three branches with noticeable flattening, a well-known feature of slow-light schemes [62]. We find a group velocity as low as 10^{-8} c for our chosen parameters. We refer the readers to Sec. IV of Ref. [39] for more details.

In practice, incoherent absorption attenuates the signal fluorescence during its propagation in the medium. This dissipative process does not imply the complete loss of energy, as it could eventually be down-converted into several lower-frequency photons and optical phonons.

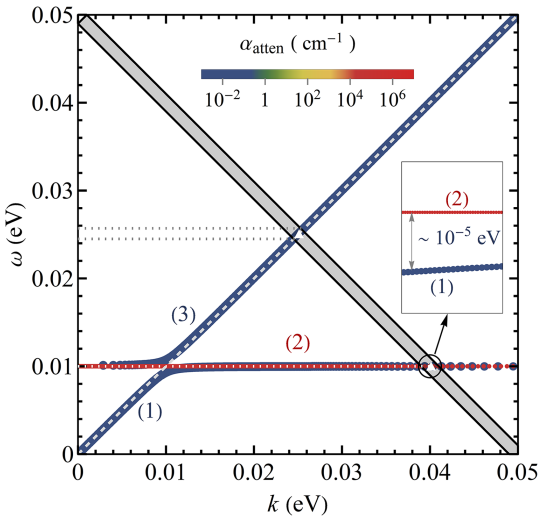


FIG. 2. The dependence curves of the photon energy ω (colorful curves) and the energy difference of neutrinos $E_3 - E_1'$ (gray band) on the photon momentum k, where $m_3 = 0.05$ eV and $m_1 = 0$ eV are inputs. The shaded gray region denotes a momentum spread of order 10^{-3} eV for illustration. The intersection points marked by white triangles represent the resultant momentum and energy satisfying the conservation law. For photons' dispersion relation, the following parameters have been used for demonstration: $E_{\rm vg} = 10$ meV, $d_{\rm vg} = e/(4m_e)$, $n_d = 6.02 \times 10^{23}$ cm^{-3}, and $T_{\rm c} = 10$ μs. Similar dispersion curves can be found in Ref. [62].

Nevertheless, such incoherent effects limit the number of ambient radiants available for neutrino coherent scatterings, which require a propagation length at least comparable to the de Broglie wavelength of the outgoing photon, i.e., $l_{\rm atten} > 1/k \sim 5$ μm. Without additional mechanisms, the attenuation length ($1/\alpha_{\rm atten}$) at the resonance peak (e.g., in the second branch in Fig. 2) for the given example is 0.03 μm, limiting the coherence application. Slight detuning from the exact resonance can significantly improve the attenuation, though at a cost of weaker resonance enhancement. In Fig. 2, the first branch near $k = 0.04$ eV corresponds to a detuning of $\Delta_{\rm p} \equiv \omega - E_{\rm vg} \approx -10^{-5}$ eV, leading to a small rate. However, we find that decreasing the dipole strength can shift this branch much closer to the resonance peak. By adopting $d_{\rm vg} = e/(250\ m_e)$, we obtain a comparable rate to Eq. (7), with a detuning -1.7×10^{-9} eV, attenuation length $l_{\rm atten} \approx 0.3$ mm and $v_{\rm g} \approx 10^{-7}$ c. For $d_{\rm vg} = e/(10^4\ m_e)$ and a reachable coherence $T_{\rm c} = 10$ ms, we obtain $R \sim 1$ yr^{-1} with $V = 10^{-3}$ m^3, $\Delta_{\rm p} \approx -10^{-12}$ eV, $l_{\rm atten} \approx 0.3$ mm and $v_{\rm g} \approx 10^{-10}$ c. Further decreasing the dipole strength will loose the flattening feature up to $k = 0.04$ eV.

It is also recognized that attenuation can be suppressed even at exact resonance through the electromagnetically induced transparency (EIT), a powerful technique widely used in slow-light experiments [52,57,65–68]. As shown in

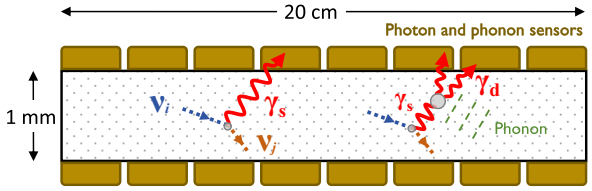


FIG. 3. A schematic plot of the experimental setup for detecting parameter fluorescence. The target is a solid film with dimensions 20 cm × 20 cm × 1 mm. Its surface is covered with superconducting photon and phonon sensors featuring $\mathcal{O}(10\ \mathrm{meV})$ sensitivities. Two types of signals can arise, depending on whether the initial photon is absorbed by the medium before reaching the sensors. Similar geometry may be found in experiments searching for light dark matters [71,72].

Ref. [39] Sec. IV, by irradiating electromagnetic waves to upper hyperfine sub-levels, e.g., separated by microwave frequencies, the medium can become transparent (with attenuation length $l_{\mathrm{atten}} > 1$ mm) to photons at the complete resonance frequency. We have not explored this effect in full detail, but a potential rate in Eq. (8) without the attenuation concern is fairly anticipated.

The target can be designed in a disc-like shape with a thickness on the $\mathcal{O}(\mathrm{mm})$ scale. A schematic of the experimental setup is shown in Fig. 3, where the target dimensions can be 20 cm × 20 cm × 1 mm. The target surface is covered with superconducting sensors sensitive to $\mathcal{O}(10)$ meV photons or phonons [69,70]. A variety of sensing technologies targeting for a few meV energy deposition are under active developments, primarily driven by the light dark matter detection [71–79]. This configuration also lends itself to stacking multiple layers. To minimize backgrounds, this device should be installed deep underground; see Ref. [39] for discussions about possible backgrounds. If signal photons reach the material surface, they can break Cooper pairs in the sensor's absorber, generating readout signals. During propagation, these photons may further interact with the material, down-converted into secondary photons and phonons, which are also detectable. Nonetheless, this requires dedicated simulations given a specific material.

Summary and discussion—In analogy to nonlinear optics, neutrinos can experience the parametric fluorescence in material targets with a photon spontaneously emitted. This process is governed by the standard weak interaction of neutrinos and does not rely on any electromagnetic couplings of neutrinos in vacuum. The basic condition is no more than the presence of clean bulk material at low temperatures. The signal is an infrared photon from the dark medium environment. By coherently interacting with this material, neutrinos can develop a rather strong effective coupling to the electromagnetic field [e.g., Eq. (4)]. The strength of this coupling depends largely on the detailed configurations of atomic or molecular energy levels of the material. A notable scenario is the resonance fluorescence, which occurs when the energy transferred by the neutrino matches the dipole frequency. The event rate of $\nu_3 \to \nu_1\gamma$ on resonance is considerable for the M1 transition. In the conservative case with the coherence time $T_c = 10$ ns, we have $R \sim 1\ \mathrm{yr}^{-1}$ for a target volume $V = 5\ \mathrm{m}^3$. In an achievable case with $T_c = 10\ \mu$s, we only need $V = 40\ \mathrm{cm}^3$ to have a rate $R \sim 8\ \mathrm{yr}^{-1}$.

We further remark on additional possible enhancement of the event rate, even though prolonging the coherence timescale already represents a promising direction. The transition rate under consideration is governed by the magnitudes of the neutrino and electron currents. In the case of the M1 transition, the neutrino current is of order one, while the electron current is suppressed by a factor of $\alpha^2 \sim 5 \times 10^{-5}$. Conversely, for the E1 transition, the suppression factor $m_i^2 a_0^2 \sim 10^{-10}$ appears in the neutrino current instead while the electron current is not suppressed. This indicates configuration mixing as a potential opportunity for significant enhancement through configuration mixing between opposite parities [80]. Parity mixing renders the transition to simultaneously proceed through both E1 and M1 channels, thus evading the suppression that individually affects each mode. Configuration mixing can be achieved with many methods, such as the Stark effect in the presence of an external electric field. The Stark effect has been extensively employed in experiments probing atomic parity violation [81,82], owing to its ability to induce sizable parity mixing. For a full parity mixing [83], we could have an enhancement factor up to $\sim 10^4$ compared to the pure M1 case. Another possible consideration is using the superradiance of a Λ-like system, where the successive transitions are of M1 and E1 types, respectively, with the neutrino coupling to the first transition and the photon coupling to the second. The superradiance mechanism itself has already been considered as an enhancement method to probe neutrino physics [84–92], including the absolute scale of neutrino masses first proposed in Ref. [93] as well as relic neutrinos [94,95].

The detection of relic neutrinos can also help to pin down basic neutrino properties, such as the absolute scale of neutrino masses and the Majorana nature. Besides relic neutrinos, the parametric fluorescence mechanism explored in the present work may also be applied to the atomic detection of dark matter [96–100] and other monoenergetic neutrino fluxes such as Mössbauer neutrinos. To make the detection concept feasible, several challenges must be addressed, including identifying suitable materials among a broad range of atoms or molecules, coherence time controlling, infrared photon or phonon sensing, and background reduction. Achieving this goal will call for joint efforts and expertise from both the particle and AMO physics communities. Since the main purpose of this work is to put forward a promising direction for relic neutrino detection, its ultimate experimental realization will be addressed in future works.

Acknowledgments—The authors would like to thank Wei Chao, Christina Gao, and Shao-Feng Ge for helpful discussions and comments. This work is supported in part by the "CUG Scholar" Scientific Research Funds at China University of Geosciences (Wuhan) under Project No. 2024014, and by the National Natural Science Foundation of China under Grants No. 12475113 and No. 12405130.

Data availability—No data were created or analyzed in this study.

[1] N. Aghanim *et al.* (Planck Collaboration), Planck 2018 results. VI. Cosmological parameters, Astron. Astrophys. **641**, A6 (2020); **652**, C4(E) (2021).
[2] S. Weinberg, Universal neutrino degeneracy, Phys. Rev. **128**, 1457 (1962).
[3] E. Baracchini *et al.* (PTOLEMY Collaboration), PTOLEMY: A proposal for thermal relic detection of massive neutrinos and directional detection of MeV dark matter, arXiv:1808.01892.
[4] M. G. Betti *et al.* (PTOLEMY Collaboration), Neutrino physics with the PTOLEMY project: Active neutrino properties and the light sterile case, J. Cosmol. Astropart. Phys. 07 (2019) 047.
[5] A. Apponi *et al.* (PTOLEMY Collaboration), Heisenberg's uncertainty principle in the PTOLEMY project: A theory update, Phys. Rev. D **106**, 053002 (2022).
[6] Y. Cheipesh, V. Cheianov, and A. Boyarsky, Navigating the pitfalls of relic neutrino detection, Phys. Rev. D **104**, 116004 (2021).
[7] Y. Cheipesh, I. Ridkokasha, V. Cheianov, and A. Boyarsky, Can we really detect relic neutrinos?, SciPost Phys. Proc. **12**, 042 (2023).
[8] R. Opher, Coherent scattering of cosmic neutrinos, Astron. Astrophys. **37**, 135 (1974), https://ui.adsabs.harvard.edu/abs/1974A&A....37../abstract.
[9] R. R. Lewis, Coherent detector for low-energy neutrinos, Phys. Rev. D **21**, 663 (1980).
[10] Y. B. Zeldovich and M. Y. Khlopov, The neutrino mass in elementary particle physics and in big bang cosmology, Sov. Phys. Usp. **24**, 755 (1981).
[11] N. Cabibbo and L. Maiani, The vanishing of order G mechanical effects of cosmic massive neutrinos on bulk matter, Phys. Lett. **114B**, 115 (1982).
[12] B. F. Shvartsman, V. B. Braginsky, S. S. Gershtein, Y. B. Zeldovich, and M. Y. Khlopov, Possibility of detecting relic massive neutrinos, JETP Lett. **36**, 277 (1982), http://jetpletters.ru/ps/1334/article_20164.shtml.
[13] P. Langacker, J. P. Leveille, and J. Sheiman, On the detection of cosmological neutrinos by coherent scattering, Phys. Rev. D **27**, 1228 (1983).
[14] P. F. Smith and J. D. Lewin, Coherent interaction of galactic neutrinos with material targets, Phys. Lett. **127B**, 185 (1983).
[15] R. R. Lewis, Radiation pressure of neutrinos in refracting media, Phys. Rev. D **35**, 2134 (1987).
[16] A. Loeb and G. D. Starkman, A detector for the cosmic neutrino background, Nucl. Phys. B, Proc. Suppl. **19**, 241 (1991).
[17] I. Ferreras and I. Wasserman, Feasibility of observing mechanical effects of cosmological neutrinos, Phys. Rev. D **52**, 5459 (1995).
[18] C. Hagmann, Cosmic neutrinos and their detection, in *American Physical Society (APS) Meeting of the Division of Particles and Fields (DPF 99)* (1999), arXiv:astro-ph/9905258.
[19] G. Duda, G. Gelmini, and S. Nussinov, Expected signals in relic neutrino detectors, Phys. Rev. D **64**, 122001 (2001).
[20] G. B. Gelmini, Prospect for relic neutrino searches, Phys. Scr. T **121**, 131 (2005).
[21] A. Ringwald, Prospects for the direct detection of the cosmic neutrino background, Nucl. Phys. **827A**, 501C (2009).
[22] P. Vogel, How difficult it would be to detect cosmic neutrino background?, AIP Conf. Proc. **1666**, 140003 (2015).
[23] V. Domcke and M. Spinrath, Detection prospects for the cosmic neutrino background using laser interferometers, J. Cosmol. Astropart. Phys. 06 (2017) 055.
[24] J. D. Shergold, Updated detection prospects for relic neutrinos using coherent scattering, J. Cosmol. Astropart. Phys. 11 (2021) 052.
[25] A. Ruzi, S. Qian, T. Yang, and Q. Li, Low energy neutrino and mass dark matter detection using freely falling atoms, arXiv:2302.09874.
[26] F. An *et al.* (JUNO Collaboration), Neutrino physics with JUNO, J. Phys. G **43**, 030401 (2016).
[27] A. Abusleme *et al.* (JUNO Collaboration), Potential to identify neutrino mass ordering with reactor antineutrinos at JUNO, Chin. Phys. C **49**, 033104 (2025).
[28] B. Abi *et al.* (DUNE Collaboration), Deep underground neutrino experiment (DUNE), far detector technical design report, volume I introduction to DUNE, J. Instrum. **15**, T08008 (2020).
[29] B. Abi *et al.* (DUNE Collaboration), Deep underground neutrino experiment (DUNE), far detector technical design report, volume II: DUNE physics, arXiv:2002.03005.
[30] K. Homma, Y. Kirita, T. Miyamaru, T. Hasada, and A. Kodama, Opening a meV mass window for axionlike particles with a microwave-laser-mixed stimulated resonant photon collider, Phys. Rev. D **110**, 092017 (2024).
[31] S. H. Kim *et al.*, Development of superconducting tunnel junction far-infrared photon detector for cosmic background neutrino decay search—COBAND experiment, Proc. Sci. ICHEP2018 (**2019**) 427.
[32] J. J. A. Baselmans *et al.*, A kilo-pixel imaging system for future space based far-infrared observatories using microwave kinetic inductance detectors, Astron. Astrophys. **601**, A89 (2017).
[33] P. M. Echternach, B. J. Pepper, T. Reck, and C. M. Bradford, Single photon detection of 1.5 THz radiation with the quantum capacitance detector, Nat. Astron. **2**, 90 (2018).
[34] R. W. Boyd, *Nonlinear Optics, Third Edition* (Academic Press, Inc., USA, 2008).

[35] D. N. Klyshko, *Photons and Nonlinear Optics*, 1st Edition (CRC Press, New York, USA, 1988).

[36] P. N. Butcher and D. Cotter, *The Elements of Nonlinear Optics*, Cambridge Studies in Modern Optics (Cambridge University Press, Cambridge, England, 1990).

[37] Y. Shih, Entangled biphoton source—property and preparation, Rep. Prog. Phys. **66**, 1009 (2003).

[38] E. Akhmedov, G. Arcadi, M. Lindner, and S. Vogl, Coherent scattering and macroscopic coherence: Implications for neutrino, dark matter and axion detection, J. High Energy Phys. 10 (2018) 045.

[39] See Supplemental Material at http://link.aps.org/supplemental/10.1103/f4zt-bbzv for the derivation procedure in the pure electromagnetic processes, more details of the relevant Hamiltonian, the result of the E1 transition, more details of the slow-light phenomenon, which includes Refs. [40–44], and discussions about possible backgrounds, which includes Refs. [45–51].

[40] X. Li, L. Zhang, L. Yang, X. Feng, L. Han, G. Fu, N. B. Manson, and C. Wei, Control an electromagnetically induced transparence feature with a microwave field, in *Quantum Optics and Applications in Computing and Communications II* (SPIE, Bellingham, Washington, USA, 2005), Vol. 5631, pp. 205–213.

[41] H. Li, V. A. Sautenkov, Y. V. Rostovtsev, G. R. Welch, P. R. Hemmer, and M. O. Scully, Electromagnetically induced transparency controlled by a microwave field, Phys. Rev. A **80**, 023820 (2009).

[42] T. Vogt, C. Gross, T. F. Gallagher, and W. Li, Microwave-assisted Rydberg electromagnetically induced transparency, Opt. Lett. **43**, 1822 (2018).

[43] D. Kosachiov and E. Korsunsky, Efficient microwave-induced optical frequency conversion, Eur. Phys. J. D **11**, 457 (2000).

[44] C. Basler, J. Grzesiak, and H. Helm, Radio-frequency-assisted electromagnetically induced transparency, Phys. Rev. A **92**, 013809 (2015).

[45] M. Baryakhtar, J. Huang, and R. Lasenby, Axion and hidden photon dark matter detection with multilayer optical haloscopes, Phys. Rev. D **98**, 035006 (2018).

[46] P. Du, D. Egana-Ugrinovic, R. Essig, and M. Sholapurkar, Sources of low-energy events in low-threshold dark-matter and neutrino detectors, Phys. Rev. X **12**, 011009 (2022).

[47] D. Baxter *et al.*, Snowmass2021 cosmic frontier white paper: Calibrations and backgrounds for dark matter direct detection, arXiv:2203.07623.

[48] R. Essig, J. Pérez-Ríos, H. Ramani, and O. Slone, Direct detection of spin-(in)dependent nuclear scattering of sub-GeV dark matter using molecular excitations, Phys. Rev. Res. **1**, 033105 (2019).

[49] Z. Guo *et al.* (JNE Collaboration), Muon flux measurement at China Jinping Underground Laboratory, Chin. Phys. C **45**, 025001 (2021).

[50] S. Derenzo, R. Essig, A. Massari, A. Soto, and T.-T. Yu, Direct detection of sub-GeV dark matter with scintillating targets, Phys. Rev. D **96**, 016026 (2017).

[51] S. Derenzo, E. Bourret, S. Hanrahan, and G. Bizarri, Cryogenic scintillation properties of *n*-type GaAs for the direct detection of MeV/c^2 dark matter, J. Appl. Phys. **123**, 114501 (2018).

[52] M. Fleischhauer, A. Imamoglu, and J. P. Marangos, Electromagnetically induced transparency: Optics in coherent media, Rev. Mod. Phys. **77**, 633 (2005).

[53] E. Fraval, M. J. Sellars, and J. J. Longdell, Method of extending hyperfine coherence times in $Pr^{3+}:Y_2SiO_5$, Phys. Rev. Lett. **92**, 077601 (2004).

[54] N. Bar-Gill, L. M. Pham, A. Jarmola, D. Budker, and R. L. Walsworth, Solid-state electronic spin coherence time approaching one second, Nat. Commun. **4**, 1743 (2013).

[55] E. Herbschleb, H. Kato, Y. Maruyama, T. Danjo, T. Makino, S. Yamasaki, I. Ohki, K. Hayashi, H. Morishita, M. Fujiwara *et al.*, Ultra-long coherence times amongst room-temperature solid-state spins, Nat. Commun. **10**, 3766 (2019).

[56] S. Upadhyay, U. Dargyte, D. Patterson, and J. D. Weinstein, Ultralong spin-coherence times for rubidium atoms in solid parahydrogen via dynamical decoupling, Phys. Rev. Lett. **125**, 043601 (2020).

[57] E. Kuznetsova, O. Kocharovskaya, P. Hemmer, and M. O. Scully, Atomic interference phenomena in solids with a long-lived spin coherence, Phys. Rev. A **66**, 063802 (2002).

[58] L. Caldwell, H. Williams, N. Fitch, J. Aldegunde, J. M. Hutson, B. Sauer, and M. Tarbutt, Long rotational coherence times of molecules in a magnetic trap, Phys. Rev. Lett. **124**, 063001 (2020).

[59] G. Heinze, C. Hubrich, and T. Halfmann, Stopped light and image storage by electromagnetically induced transparency up to the regime of one minute, Phys. Rev. Lett. **111**, 033601 (2013).

[60] L. V. Hau, S. E. Harris, Z. Dutton, and C. H. Behroozi, Light speed reduction to 17 metres per second in an ultracold atomic gas, Nature (London) **397**, 594 (1999).

[61] R. S. T. Jacob B. Khurgin, *Slow Light: Science and Applications*, 1st ed., Optical Science and Engineering (CRC Press, New York, USA, 2008).

[62] J. B. Khurgin, Slow light in various media: A tutorial, Adv. Opt. Photonics **2**, 287 (2010).

[63] A. Turukhin, V. Sudarshanam, M. Shahriar, J. Musser, B. Ham, and P. Hemmer, Observation of ultraslow and stored light pulses in a solid, Phys. Rev. Lett. **88**, 023602 (2001).

[64] D. Schraft, M. Hain, N. Lorenz, and T. Halfmann, Stopped light at high storage efficiency in a $Pr^{3+}:Y_2SiO_5$ crystal, Phys. Rev. Lett. **116**, 073602 (2016).

[65] S. E. Harris, Electromagnetically induced transparency, Phys. Today **50**, No. 7, 36 (1997).

[66] J. P. Marangos, Electromagnetically induced transparency, J. Mod. Opt. **45**, 471 (1998).

[67] M. Lukin and A. Imamoğlu, Controlling photons using electromagnetically induced transparency, Nature (London) **413**, 273 (2001).

[68] R. Finkelstein, S. Bali, O. Firstenberg, and I. Novikova, A practical guide to electromagnetically induced transparency in atomic vapor, New J. Phys. **25**, 035001 (2023).

[69] S. R. Golwala and E. Figueroa-Feliciano, Novel quantum sensors for light dark matter and neutrino detection, Annu. Rev. Nucl. Part. Sci. **72**, 419 (2022).

[70] R. Essig *et al.*, Snowmass2021 cosmic frontier: The landscape of low-threshold dark matter direct detection

in the next decade, in Snowmass 2021 (2022), arXiv:2203.08297.
[71] D. J. Temples *et al.*, Performance of a phonon-mediated kinetic inductance detector at the NEXUS cryogenic facility, Phys. Rev. Appl. **22**, 044045 (2024).
[72] D. J. Temples *et al.*, Development status of the KIPM detector consortium, arXiv:2509.25544.
[73] S. A. Lyon, K. Castoria, E. Kleinbaum, Z. Qin, A. Persaud, T. Schenkel, and K. M. Zurek, Single phonon detection for dark matter via quantum evaporation and sensing of ^{3}He, Phys. Rev. D **109**, 023010 (2024).
[74] A. Cruciani *et al.*, BULLKID: Monolithic array of particle absorbers sensed by kinetic inductance detectors, Appl. Phys. Lett. **121**, 213504 (2022).
[75] J. Gao, Y. Hochberg, B. V. Lehmann, S. W. Nam, P. Szypryt, M. R. Vissers, and T. Xu, Detecting light dark matter with kinetic inductance detectors.
[76] K. Ramanathan, J. E. Parker, L. M. Joshi, A. D. Beyer, P. M. Echternach, S. Rosenblum, B. J. Sandoval, and S. R. Golwala, Quantum parity detectors: A qubit based particle detection scheme with meV thresholds for rare-event searches, arXiv:2405.17192.
[77] L. Baudis *et al.*, First sub-MeV dark matter search with the QROCODILE experiment using superconducting nanowire single-photon detectors, Phys. Rev. Lett. **135**, 081002 (2025).
[78] T. K. Bui *et al.* (TESSERACT Collaboration), First limits on light dark matter interactions in a low threshold two-channel athermal phonon detector from the TESSERACT Collaboration, Phys. Rev. Lett. **135**, 161002 (2025).
[79] B. J. Sandoval, A. D. Beyer, P. M. Echternach, S. R. Golwala, W. D. Ho, L. Yuan, and K. Ramanathan, Assessing the operating characteristics of an ion-milled phonon-mediated quantum parity detector, arXiv:2509.18637.
[80] B. Bransden and C. Joachain, *Physics of Atoms and Molecules* (Dorling Kindersley Pvt Ltd, London, England, 2006).
[81] M. A. Bouchiat and C. Bouchiat, Parity violation induced by weak neutral currents in atomic physics. Part 2, J. Phys. II (France) **36**, 493 (1975).
[82] M. Bouchiat, J. Guena, L. Hunter, and L. Pottier, Observation of a parity violation in cesium, Phys. Lett. **117B**, 358 (1982).
[83] S. Gong, P. Wang, and Y. Mo, Electric-field-induced mixing of opposite parity states: Insights from spectra of the CO (b3Σ+ ← a3ΠΩ) transition, Phys. Rev. A **110**, 052801 (2024).
[84] A. Fukumi *et al.*, Neutrino spectroscopy with atoms and molecules, Prog. Theor. Exp. Phys. **2012**, 04D002 (2012).
[85] M. Yoshimura, N. Sasao, and M. Tanaka, Dynamics of paired superradiance, Phys. Rev. A **86**, 013812 (2012).
[86] D. N. Dinh, S. T. Petcov, N. Sasao, M. Tanaka, and M. Yoshimura, Observables in neutrino mass spectroscopy using atoms, Phys. Lett. B **719**, 154 (2013).
[87] N. Song, R. Boyero Garcia, J. J. Gomez-Cadenas, M. C. Gonzalez-Garcia, A. Peralta Conde, and J. Taron, Conditions for statistical determination of the neutrino mass spectrum in radiative emission of neutrino pairs in atoms, Phys. Rev. D **93**, 013020 (2016).
[88] J. Zhang and S. Zhou, Improved statistical determination of absolute neutrino masses via radiative emission of neutrino pairs from atoms, Phys. Rev. D **93**, 113020 (2016).
[89] G.-Y. Huang, N. Sasao, Z.-Z. Xing, and M. Yoshimura, Testing unitarity of the 3×3 neutrino mixing matrix in an atomic system, Int. J. Mod. Phys. A **35**, 2050004 (2020).
[90] S.-F. Ge and P. Pasquini, Probing light mediators in the radiative emission of neutrino pair, Eur. Phys. J. C **82**, 208 (2022).
[91] S.-F. Ge and P. Pasquini, Unique probe of neutrino electromagnetic moments with radiative pair emission, Phys. Lett. B **841**, 137911 (2023).
[92] S.-F. Ge and P. Pasquini, Disentangle neutrino electromagnetic properties with atomic radiative pair emission, J. High Energy Phys. 12 (2023) 083.
[93] M. Yoshimura, Neutrino pair emission from excited atoms, Phys. Rev. D **75**, 113007 (2007).
[94] M. Yoshimura, N. Sasao, and M. Tanaka, Experimental method of detecting relic neutrino by atomic de-excitation, Phys. Rev. D **91**, 063516 (2015).
[95] A. Arvanitaki, S. Dimopoulos, and M. Galanis, Superradiant interactions of the cosmic neutrino background, axions, dark matter, and reactor neutrinos, Phys. Rev. D **111**, 055015 (2025).
[96] M. S. Safronova, D. Budker, D. DeMille, D. F. J. Kimball, A. Derevianko, and C. W. Clark, Search for new physics with atoms and molecules, Rev. Mod. Phys. **90**, 025008 (2018).
[97] A. Arvanitaki, S. Dimopoulos, and K. Van Tilburg, Resonant absorption of bosonic dark matter in molecules, Phys. Rev. X **8**, 041001 (2018).
[98] G.-Y. Huang and S. Zhou, Probing cosmic axions through resonant emission and absorption in atomic systems with superradiance, Phys. Rev. D **100**, 035010 (2019).
[99] A. Bhoonah, J. Bramante, and N. Song, Superradiant searches for dark photons in two stage atomic transitions, Phys. Rev. D **101**, 055040 (2020).
[100] M. Bauer, J. Perez-Soler, and J. D. Shergold, Generalised hydrogen interactions with CINCO: A window to new physics, J. High Energy Phys. 10 (2024) 176.